JPE 5-4-1

Analysis of an AC/DC Resonant Pulse Power Converter for Energy Harvesting Using a Micro Piezoelectric Device

Gyo-Bum Chung† and Khai D.T. Ngo*

†Dept. of Electronic and Electrical Eng., Hongik University, Jochiwon, Chungnam, Korea
*Dept. of Electrical and Computer Eng., University of Florida, Gainesville, FL, USA

ABSTRACT

In order to harvest power in an efficient manner from a micro piezoelectric (PZT) device for charging the battery of a remote system, a new AC/DC resonant pulse power converter is proposed. The proposed power converter has two stages in the power conversion process. The first stage includes N-type MOSFET full bridge rectifier. The second stage includes a boost converter having an N-type MOSFET and a P-type MOSFET. MOSFETs work in the 1st or 3rd quadrant region. A small inductor for the boost converter is assigned in order to make the size of the power converter as small as possible, which makes the on-interval of the MOSFET switch of the boost converter ultimately short. Due to this short on-interval, the parasitic junction capacitances of MOSFETs affect the performance of the power converter system. In this paper, the performance of the new converter is analytically and experimentally evaluated with consideration of the parasitic capacitance of switching devices.

Keywords: Resonance, Pulse, Energy Harvesting, Micro piezoelectric device

1. Introduction

Interest in the area of remote systems has increased[1-3]. For remote power systems, there are no means for power to be supplied through the power grid line. Therefore remote systems need batteries as energy sources. The battery must be replaced because of its limited lifetime. However, the replacement of a battery is not a good choice in some remote systems. For remote power systems, the concept of energy harvesting has been proposed and has been realized with energy storage and its own power generator which must utilize an environmental power source such as mechanical vibration, heat, sunlight, and wind. The piezoelectric (PZT) device has good characteristics for converting mechanical vibration to electric energy[4,5]. For this application, a step down buck converter and a discontinuous current mode flyback converter were considered[6]. The maximization of the power flowing from the PZT cantilever to the battery has been studied[6]. However, since the output voltage and the power of the PZT device are very small, the power converter should be designed carefully[7].

In this paper, a new power converter for energy harvesting is proposed and analyzed with consideration of the effects of the parasitic capacitances of MOSFETs. The power losses of the converter are analytically calculated. Computer simulation studies are also performed to prove

Manuscript received March 17, 2005; revised July 15, 2005
†Corresponding Author: gbchung@wow.hongik.ac.kr
Tel: +82-41-860-2412, Fax: +82-41-863-7605, Hongik Univ.
*Dept. of Electrical and Computer Eng. Univ. of Florida

the feasibility of the power converter and the loss calculation. Experimental results are explained to prove the feasibility of the proposed converter.

2. Topology

Fig. 1 shows a new AC/DC resonant pulse power converter which transfers electric energy from AC current source, I_s, to battery, V_b.

AC current source, I_s, and a capacitor, C_e, is the electrical equivalent circuit of a PZT cantilever, which converts the mechanical vibration to the electric energy. The magnitude of AC current source, I_s, is proportional to the strength of the mechanical vibration. The frequency, f_{ac}, of the AC current source is equal to the frequency of the mechanical vibration.

The power conversion process of the power converter has two stages. In the first stage, MOSFET full bridge rectifier (active rectifier) converts the AC voltage, V_{ab}, of the PZT device to DC voltage, V_{rec}. In the second stage, a boost converter converts the small DC voltage, V_{rec}, to a high battery voltage, V_b.

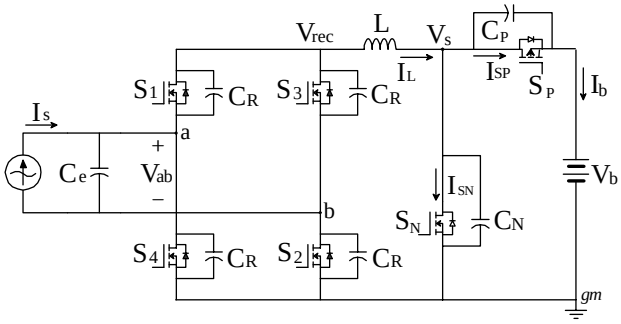

Fig. 1 Simplified converter topology

MOSFETs in the active rectifier work in the 3rd quadrant region, which reduces conduction losses in the low voltage application, compared to a diode full bridge rectifier[8]. The boost converter having a MOSFET synchronous rectifier, S_P, instead of diode also has small conduction losses. In order to reduce the physical size of the power converter, the rectifier in the first stage does not have a capacitive output filter. The smallest possible resonant inductor, L, is also chosen. Therefore, the peak value of the rectified voltage, V_{rec}, is not reduced and the resonant circuit of LC_e has a very high resonant frequency, f_r. The parasitic capacitors of MOSFETs in the converter have some effects on the converter operation in the high frequency region.

3. Operational Principle

With consideration of the parasitic drain-to-source capacitances of MOSFETs, the switching duration of the AC resonant pulse power converter for the half period of AC current source, I_s, can be divided into eight modes. The active parts of the converter for eight modes are plotted in Fig 2 and the analytical waveforms of voltages and currents in the converter are depicted in Fig. 3. The duration of mode 1, T_1 ($=t_1$-t_0), is approximately as long as the half period of the source current, I_s.

(1) Mode 1 ($t_0 \sim t_1$) : The voltage, $V_{ab}(t)$, of the capacitor, C_e, is almost zero at t_0 because its energy has been transferred to the battery in the previous half cycle of the current source, I_s. MOSFET switches (S_1, S_2) of the rectifier turn on at t_0 while the others (S_3, S_4) turn off. Since the magnitude of $V_{ab}(t)$ at t_o is almost zero, the switching loss of the active rectifier is negligibly small. The current source, I_s, begins to charge the capacitor, C_e, and the magnitude of $V_{ab}(t)$ increases positively.

(2) Mode 2 ($t_1 \sim t_2$) : When $V_{ab}(t)$ reaches the peak value at t_1, the peak voltage detector produces the turn-on signal for the MOSFET switch, S_N, of the boost converter. The energy stored in the parasitic capacitor, C_N, is discharged instantly through the MOSFET on-resistor, R_{ds}. And the parasitic capacitor, C_P, is charged up to the battery voltage, V_b.

(3) Mode 3 ($t_2 \sim t_3$) : After S_N completely turns on, the resonant current path consists of the PZT output capacitor, C_e, the resonant inductor, L, and the ohmic resistors of three MOSFETs (S_1, S_2, S_N). The resonant frequency, f_r, is approximately written as

$$f_r \approx \frac{1}{2\pi\sqrt{LC_e}} \tag{1}$$

Since the smallest possible inductance is chosen, the resonant frequency of the converter in mode 3 is very high.

$$f_r >> f_{ac} \tag{2}$$

The duration of mode 3, T_3 ($=t_3$-t_2), is approximately written as

$$T_3 = kT = \frac{1}{4 f_r} = \frac{\pi\sqrt{LC_e}}{2} \tag{3}$$

which is very short.

The energy stored in the PZT output capacitor, C_e, is rapidly transferred to the resonant inductor, L. Mode 3 ends when V_{ab} becomes zero.

(4) Mode 4 ($t_3 \sim t_4$) : Mode 4 is the deadtime interval for MOSFET S_N, starting at t_3 and ending at t_4. After S_N turns off, S_P does not turn on immediately. The parasitic capacitor, C_P, is charged up from V_b to $\frac{C_N}{C_N + C_P} V_b$ and the parasitic capacitor, C_N, is charged up from 0 [V] to $\frac{C_P}{C_N + C_P} V_b$ instantly. The inductor current, I_L, continues to flow through two parasitic capacitors C_N and C_P. Mode 4 continues until the deadtime guarantees the complete turn-off of MOSFET S_N.

(5) Mode 5 ($t_4 \sim t_5$) : MOSFET S_P turns on at t_4. The drain current of S_P increases from $-\frac{C_P}{C_N + C_P} I_L$ to $-I_L$ and the current of C_N decreases from $\frac{C_N}{C_N + C_P} I_L$ to 0 [A] instantly. With the source-to-drain voltage drop V_{ds} of S_p in the 3rd quadrant region, the voltage of C_N increases up to $V_b + V_{ds}$ instantly. Energy stored in L is transferred to the battery until the magnitude of I_L becomes zero.

(6) Mode 6 ($t_5 \sim t_6$) : MOSFET S_P turns off when $I_L(t_5)$ equals 0 at t_5. The resonant current path consists of the resonant inductor, the PZT output capacitor C_e and the parasitic capacitor C_P in parallel with C_N. The resonant inductor current, I_L, flows in the opposite direction. This mode is also for the dead time interval to guarantee the complete turn off of MOSFET S_P. Mode 6 should end before the reverse body diode of S_N turns on.

(7) Mode 7 ($t_6 \sim t_7$) : MOSFET S_N turns on at t_6 and goes into the 3rd quadrant region. The resonant circuit consists of the resonant inductor and the PZT output capacitor. After the resonant current becomes zero at t_7, MOSFET S_N turns off. The duration of Mode 7, T_7, is approximately written as

$$T_7 = \frac{1}{2 f_r} \tag{4}$$

(8) Mode 8 ($t_7 \sim t_0'$) : The resonant current path consists of the parasitic capacitors (C_P and C_N), the resonant inductor and the PZT output capacitor. The oscillation disappears slowly due to the circuit damping. This mode ends at the time of t_0', at which time the switches (S_1, S_2) of the rectifier turn off and the switches (S_3, S_4) of the rectifier turn on. Then mode 1 for the next half cycle of the current source, I_s, will be repeated.

4. Control Algorithm

In order to operate the AC/DC resonant pulse converter efficiently for energy harvesting, the control algorithm for the converter switching is developed and depicted in Fig. 4.

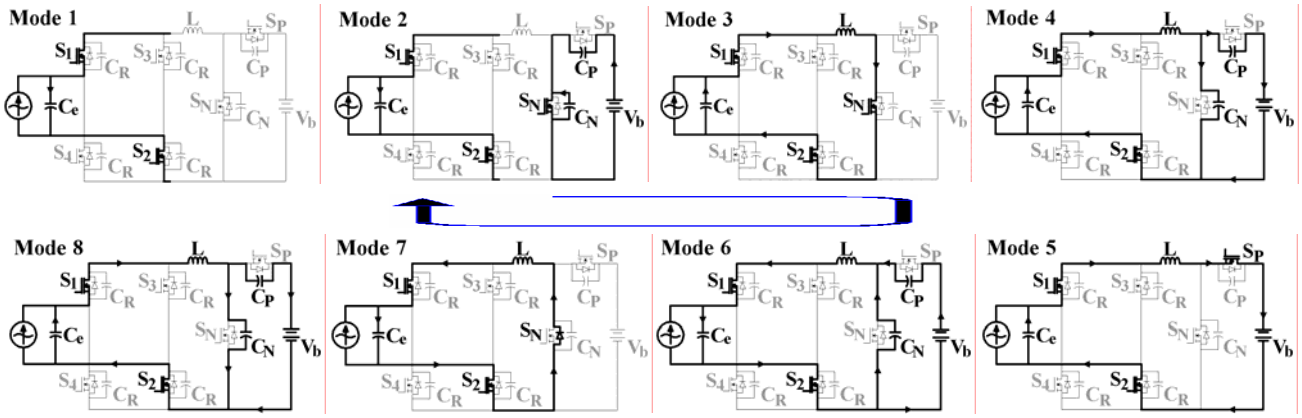

Fig. 2 Active parts of the converter for eight operational modes of AC/DC resonant pulse converter

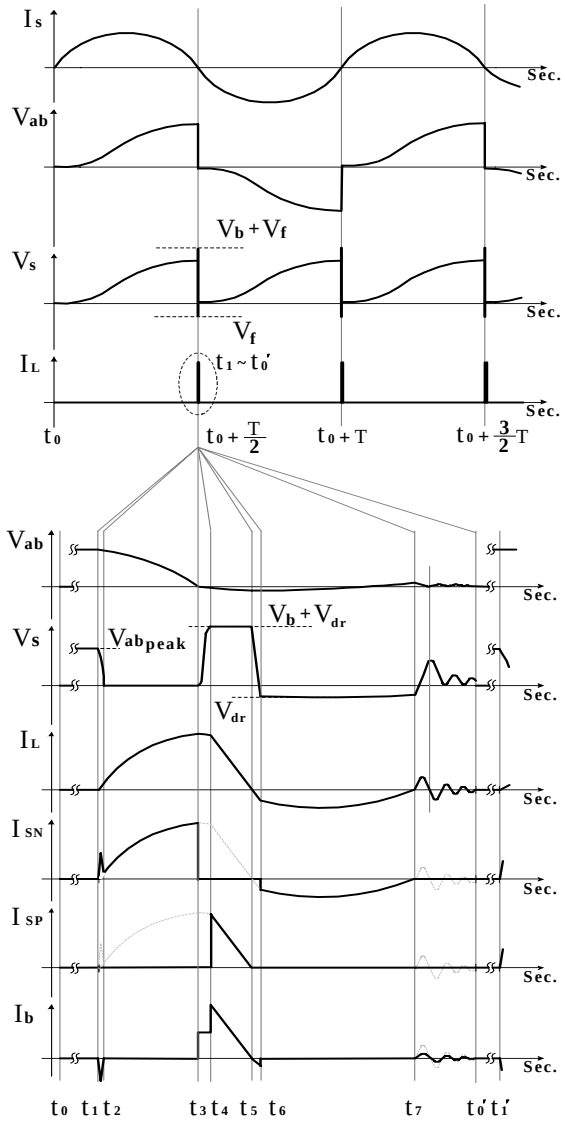

Fig. 3 Analytical voltage and current waveforms

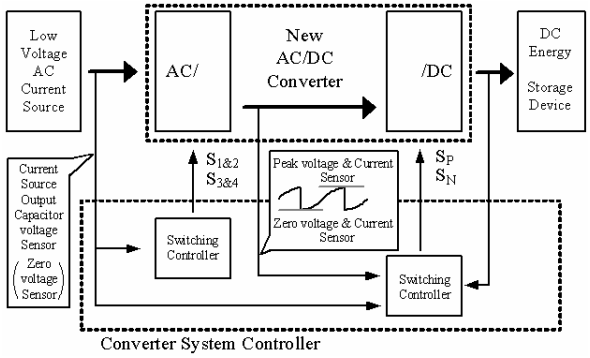

Fig. 4 Switching controller of AC/DC resonant pulse converter

The controller has the peak-voltage detector, the zero-voltage detector, the peak-current detector, the zero-current detector, and the voltage-polarity checker.

The peak voltage detector of $V_{ab}(t)$ generates a turn-on signal for S_N at t_1. The peak current detector of the resonant inductor current, I_L, generates a turn-off signal for S_N at t_3 and a turn-on signal for S_P at t_4. The zero current detector of I_L generates a turn-off signal for S_P at t_5 and a turn-on signal for S_N at t_6. The zero current detector of I_L generates a turn-off signal for S_N at t_7. The voltage-polarity checker and zero voltage detector of $V_{ab}(t)$ generate the turn-off signal (S_1 and S_2) at t_0' and the turn-on signal (S_3 and S_4) at t_0'.

5. Loss Calculation

In order to evaluate the performance of the converter proposed for energy harvesting, the energy losses in eight modes are calculated analytically and programmed in MATLAB. However, this analysis covers only the power circuit of the converter.

From Fig. 2, the current path of each mode has its own resistors, an inductor, and capacitors.

Mode 1 ($t_0 \sim t_1$) MOSFETs S_1, S_2 of the rectifier are on-state. However, the current of the AC current source, I_S, does not flow through the converter since the output capacitor, C_e is much bigger than the parasitic capacitors, C_N of S_N and C_P of S_P. Therefore, the resonant inductor current, I_L, of mode 1 is negligibly small. Therefore the energy loss of the converter in mode 1 is negligibly small.

The source current, I_S, and voltage, V_{ab}, are written as

$$V_{ab}(t) = V_m \sin(\omega t + \theta) \tag{5}$$

$$I_S(t) = I_m \sin\left(\omega t + \theta + \frac{\pi}{2}\right) \tag{6}$$

$V_{ab}(t)$ has the peak value at t_1. With consideration of the parasitic capacitors of the MOSFET rectifier, the energy stored in the output capacitor, C_e, is written as

$$W_{Ce} = \frac{1}{2}(C_e + C_N) \cdot V_m^2 \tag{7}$$

Mode 2 ($t_1 \sim t_2$) MOSFET, S_N, transits from the turn-off

state at t_1 to the turn-on state at t_2. The energy stored in the parasitic capacitor of MOSFET S_N, is discharged instantly through the MOSFET on-resistor, R_{ds}. The energy lost in mode 2 is written as

$$W_{loss,2} = \frac{1}{2} C_N \cdot V_m^2 \tag{8}$$

The voltage of the parasitic capacitor, C_P, of MOSFET S_P, is charged from V_m-V_b to -V_b instantly. The amount of energy changed in the parasitic capacitor of MOSFET S_P, is written as

$$\frac{1}{2} C_P V_b^2 - \frac{1}{2} C_P (V_b - V_m)^2 \tag{9}$$

which comes from the battery, V_b, and is not an ohmic-energy loss.

The energy stored in the output capacitor, C_e, at t_2, is the same as W_{Ce} of mode 1 .

Mode 3 ($t_2 \sim t_3$) After S_N turns on completely at t_2, the current and voltage equations are written as

$$L\frac{di_L}{dt} + R \cdot i_L + \frac{1}{C_e}\int i_L dt - V_{ab}(t_2) + 3 \cdot V_{ds} = 0 \tag{10}$$

$$V_{ab}(t) = -V_{Ce}(t) = -\frac{1}{C_e}\int_0^t i_L(\tau) d\tau + V_m \tag{11}$$

where R is MOSFET on-resistance, R_{ds}, plus the resistance of the inductor, R_L, and V_{ds} is the forward voltage drop of MOSFET.

With the initial conditions ($i_L(t_2)=0$, $V_{ab}(t_2)=V_m$, and $I_s(t_2)= 0$), the resonant current, $i_L(t)$, is written as

$$i_L(t) = \frac{-3 \cdot V_{ds} + V_m}{\omega L} e^{-\alpha t} \sin \omega t = I_m e^{-\alpha t} \sin \omega t \tag{12}$$

The capacitor voltage, $V_{ab}(t)$, is written as

$$V_{ab}(t) = \frac{-3 \cdot V_{ds} + V_m}{\omega L C_e} \frac{-1}{\sqrt{\alpha^2 + \omega^2}} e^{-\alpha\tau}(\sin[\omega t + \theta] - \sin\theta) + V_m \tag{13}$$

where $\alpha = \frac{R}{2L}$, $\omega = \sqrt{\frac{1}{L \cdot C_e} - \left(\frac{R}{2L}\right)^2}$ and $\tan^{-1}\theta = \frac{\omega}{\alpha}$.

In order to resonate the LC_e circuit, the following equation should be satisfied.

$$\sqrt{\frac{L}{C_e}} \geq \frac{R}{2} \tag{14}$$

When $V_{ab}(t)$ reaches zero voltage, mode 3 ends. The energy stored in the resonant inductor, L, at t_3 is written as

$$\frac{1}{2} L \cdot I_m^2 \tag{15}$$

The energy loss of mode 3 is written as

$$W_{loss,3} = \int_{t2}^{t3} i_L(t)^2 R \cdot dt + 3\int_{t2}^{t3} i_L(t) V_{ds} \cdot dt \tag{16}$$

Mode 4 ($t_3 \sim t_4$) During the dead time interval, the resonant current and voltage equations are written as

$$L\frac{di_L}{dt} + Ri_L + \frac{1}{C_e}\int i_L dt - V_{ab}(t_3) + \frac{1}{C_N + C_P}\int i_L dt + \frac{C_P}{C_N + C_P} V_b = 0 \tag{17}$$

$$v_{CN}(t) = \frac{1}{C_N}\int_0^t \frac{C_N}{C_N + C_P} i_L(\tau) d\tau + \frac{C_P}{C_N + C_P} V_b \tag{18}$$

where $R = 2 \cdot R_{ds} + R_L + \frac{C_P}{C_N + C_P} R_b$, and $V_{ab}(t_3)$ is calculated at t_3 in mode 3.

The energy losses of mode 4 are written as

$$W_{R,4} = \int_{t3}^{t4} i_L(t)^2 R \cdot dt = \int_0^{\Delta t} i_L(t)^2 (2 \cdot R_{ds} + R_L + \left(\frac{C_D}{C_p + C_D}\right)^2 R_b) \cdot dt \tag{19}$$

$$W_{S,4} = \int_{t3}^{t4} 2 \cdot V_{ds} \cdot i_L(\tau) dt = \int_0^{\Delta t} 2 \cdot V_{ds} \cdot i_L(\tau) dt \tag{20}$$

where $\Delta t = t_4 - t_3$

The energy transferred to the battery is written as

$$W_{H,4} = \int_0^{\Delta t} V_b \frac{C_P}{C_N + C_P} i_L(\tau) \cdot dt \tag{21}$$

Since the interval of mode 4 is very short and the impedance of the resonant current path is very high, the energy loss is negligible.

Mode 5 ($t_4 \sim t_5$) After MOSFET S_P turns on completely at t_4, the resonant current equation is written as

$$L\frac{di_L}{dt} + Ri_L + \frac{1}{C_e}\int i_L(t) dt - V_{ab}(t_4) + V_b + 3 \cdot V_{ds} = 0 \tag{22}$$

where $V_{ab}(t_4) = V_{Ce}(t_4) \approx 0$, $i_L(t=t_4) = i_L(0) \approx I_m$ and $R = 3 \cdot R_{ds} + R_L$.

The resonant current $i_L(t)$ is written as

$$i(t) = e^{-\alpha t}\left(A_1 \cos \omega t + A_2 \sin \omega t\right) \tag{23}$$

where $A_1 = I_m$ and $A_2 = \frac{-V_b - 3 \cdot V_{ds} - R \cdot I_m + \alpha L \cdot I_m}{\omega L}$.

Then, the energy loss of mode 5 is written as

$$W_{loss,5} = \int_{t4}^{t5}\left(i_L(t)^2 R + 3V_{ds} \cdot i_L(t)\right)dt \tag{24}$$

And the energy transferred to the battery is written as

$$W_{H,5} = \int_{t4}^{t5} V_b \cdot i_L(t)dt \tag{25}$$

Mode 6 (t_5 ~ t_6) During the dead time interval for MOSFET S_P, the resonant current and voltage equations are written as

$$L\frac{di_{L1}}{dt} + Ri_{L1} + \frac{1}{C_e}\int i_{L1}dt + V_{ab}(t_5) + \frac{1}{C_N + C_P}\int i_{L1}dt + \frac{C_P}{C_N + C_P}V_b = 0 \tag{26}$$

$$v_{CN}(t) = -\frac{1}{C_N}\int_0^t \frac{C_N}{C_N + C_P} i_{L1} d\tau + \frac{C_P}{C_N + C_P} V_b \tag{27}$$

where $R = 2 \cdot R_{ds} + R_L + \frac{C_P}{C_N + C_P} R_b$.

The direction of i_{L1} in mode 6 is opposite to the direction of i_L in mode 3. $V_{ab}(t_5)$ is calculated at t_5 in mode 5.

The energy losses of mode 6 are written as

$$W_{R,6} = \int_{t5}^{t6} i_L(t)^2 R \cdot dt = \int_0^{\Delta t} i_L(t)^2 \left(2 \cdot R_{ds} + R_L + \left(\frac{C_D}{C_p + C_D}\right)^2 R_b\right) \cdot dt \tag{28}$$

$$W_{S,5} = \int_{t5}^{t6} 2 \cdot V_{ds} \cdot i_L(t)dt = \int_0^{\Delta t} 2 \cdot V_{ds} \cdot i_L(t)dt \tag{29}$$

where $\Delta t = t_6 - t_5$

The energy transferred to the battery is written as

$$W_{H,6} = -\int_0^{\Delta t} V_b \frac{C_P}{C_N + C_P} I_{L1} \cdot dt \tag{30}$$

Since mode 6 is as short as mode 4, the energy loss is negligible.

Mode 7 (t_6 ~ t_7) In the 3rd quadrant region of MOSFETs(S_1, S_2, S_N), the current and voltage equations are written as

$$L\frac{di_{L1}}{dt} + R \cdot i_{L1} + \frac{1}{C_e}\int i_{L1}dt + V_{ab}(t_6) + 3 \cdot V_{ds} = 0 \tag{31}$$

$$V_{ab}(t) = \frac{1}{C_e}\int_0^t i_{L1}(\tau)d\tau + V_{ab}(t_6) \tag{32}$$

The energy loss is written as

$$W_{loss,7} = \int_0^{\Delta t} i_L(t)^2 (3 \cdot R_{ds} + R_L) \cdot dt + \int_0^{\Delta t} i_L(t) \cdot 3 \cdot V_{ds} \cdot dt \tag{33}$$

Mode 8 (t_7 ~ t_8) The resonant current and voltage equations with the initial condition of $i_L(t_7)=0$ are written as

$$L\frac{di_L}{dt} + Ri_L + \frac{1}{C_e}\int i_L dt - V_{ab}(t_7) + \frac{1}{C_N + C_P}\int i_L dt + \frac{C_P}{C_N + C_P}V_b = 0 \tag{34}$$

$$V_{ab}(t) = \frac{1}{C_e}\int_0^t i_L(\tau)d\tau - V_{ab}(t_7) \tag{35}$$

where $R = 2 \cdot R_{ds} + R_L + R_b$.

The energy loss is written as

$$W_{loss,8} = \int_0^{\Delta t}\left(i_L(t)^2 R + 2V_{ds} i_L(t)\right)dt \tag{36}$$

The energy transferred to the battery is written as

$$W_{H,8} = \int_0^{\Delta t} V_b \frac{C_P}{C_N + C_P} i_L(t) \cdot dt \tag{37}$$

where $\Delta t = t_8 - t_7 = 10\tau = 10\frac{1}{\alpha}$

Total Energy Loss : The energy loss, W_{loss}, for the half period of the current source, I_s, is the sum of the ohmic loss, $W_{R,n}$, and the switching loss, $W_{S,n}$, for n mode.

$$W_{loss} = \sum_1^8 \left(W_{R,n} + W_{S,n}\right) = \sum_1^8 \left(\int_{t_{n-1}}^{t_n} i_n^2(t) R_n dt + \int_{t_{n-1}}^{t_n} V_{tn} i_n(t)dt\right) \tag{38}$$

where R_n is the equivalent resistance and V_{tn} is the equivalent turn-on voltage drop of switches for mode n.

6. Simulation and Calculations

A simulation study using PSIM is performed to prove the existence of eight operational modes. The simulation generates a great amount of data because of the ultimately short turn-on interval. For the purpose of proving that eight operational modes exist in the half cycle of the AC source, the frequency of the AC current source in Fig.1 is set to 31240[Hz]. The parameters of the converter in the simulation study are as follows: I_s=200[μA], f_{ac}=31240[Hz], C_e=582.6[nF], L=2[μH], the resistance of inductor=1[Ω], C_N=C_P=C_R=3[pF], V_b=5[V], MOSFET R_{ds}=3[Ω], and MOSFET reverse diode forward voltage drop V_{SD}=0.7[V].

Fig. 5 shows the PZT voltage, V_{ab}, the rectified voltage, V_{rec}, and the inductor current, I_L, of the converter. The switching period of S_N is 16[μsec]. As the turn-on interval of MOSFET S_N is ultimately short, the inductor current I_L looks like a pulse. The efficiency of the converter from Fig. 5(d) is 65.5% in the PSIM simulation and 61.5% is calculated in MATLAB program of the loss calculation. The difference in the efficiencies comes from the approximation used in the loss analysis

Fig. 6 shows the current waveforms depicted in the enlarged time scale, which is the circled area of Fig. 5. Fig. 6 shows the existence of eight operational modes in the every half cycle of the current source, I_s. The turn-on interval of MOSFET S_N is (t_1-t_3), which is as ultimately short as 51[nsec]. The turn-on interval of MOSFET S_P in mode 5 is (t_4-t_5), which is as short as 17.4[nsec]. The voltage, V_s, in Fig. 6(b) shows the resonant frequency due to L and the parasitic capacitors, C_P or C_N after t_7. The inductor current, I_L, in Fig. 6(c) shows the resonant frequency due to L and C_e. Fig. 6(d) shows that MOSFET S_N turns on in the 3rd quadrant region for (t_6-t_7). Mode 7 is as short as 94.3[nsec]. Fig. 6(f) shows the waveform of I_b, which transfers the energy to the battery.

Fig. 7 shows the transferred energies calculated with consideration of the parasitic capacitances. The bar of C_N=3[pF] in Fig. 7 is the energy ratio transferred to the battery for C_P =3, 6, 9, 12, 15 [pF] with the constant value of C_N=3[pF]. And the bar of C_P =3[pF] is the energy ratio transferred to the battery for C_N =3, 6, 9, 12, 15 [pF] with the constant value of C_P=3[pF]. The converter transfers 49% of the energy stored in C_e at t_0 to the battery with C_P=3[pF] and C_N=3[pF]. The analytical calculation of the energy loss is equal to the results of the PSIM simulation, in which energy can be measured with a voltage sensor, a current sensor, a multiplier and an integrator. Fig. 7 also shows that the greater the parasitic capacitances are, the worse the converter efficiency is. C_p of S_P has a worse effect on the converter efficiency than C_N of S_N.

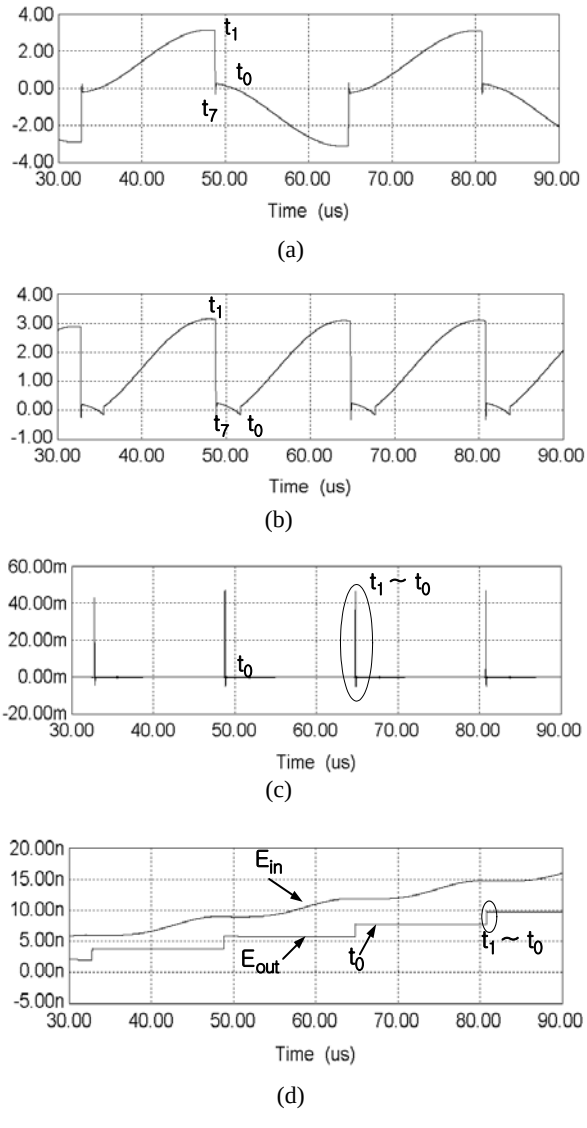

Fig. 5 Simulated Current Waveforms of AC/DC converter (a) voltage of the output capacitor of the current source V_{ab} (b) rectifier output voltage V_{rec} (c) inductor current I_L (d) Supplied energy E_{in} and harvested energy E_{out}.

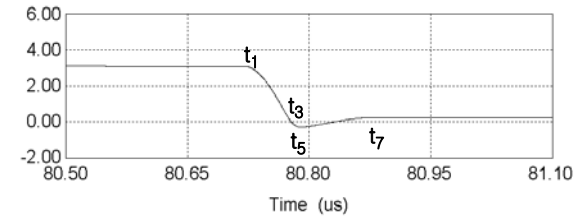

(a)

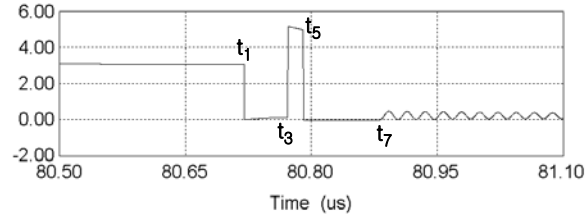

(b)

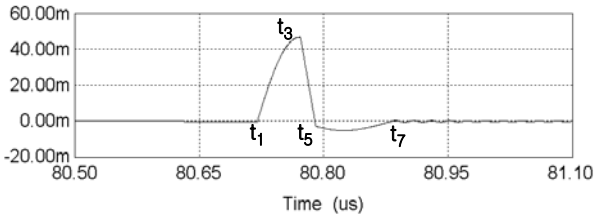

(c)

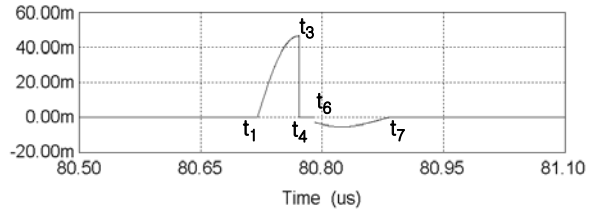

(d)

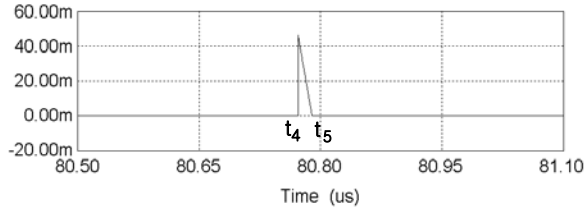

(e)

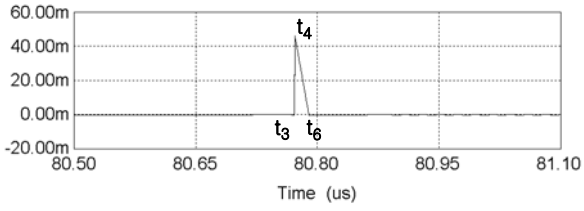

(f)

Fig. 6 Simulated Current Waveforms of the AC/DC Converter in an enlarged time scale
(a) Vrec (b) Vs (c) IL (d) ISN (e) ISP (f) Ib

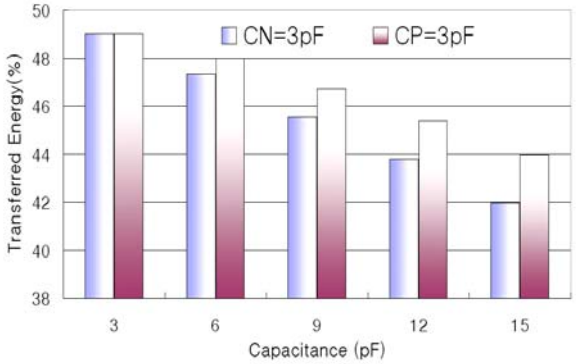

Fig. 7 Transferred energy from capacitor Ce to battery Vb versus the parasitic capacitances

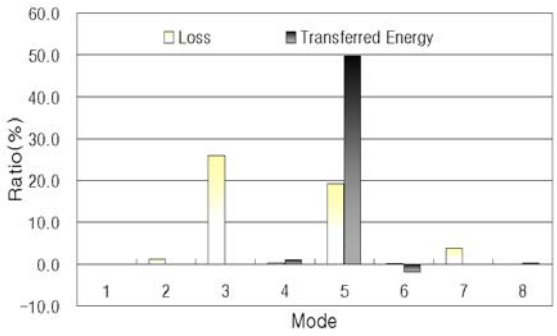

Fig. 8 Lost and transferred energies for eight modes

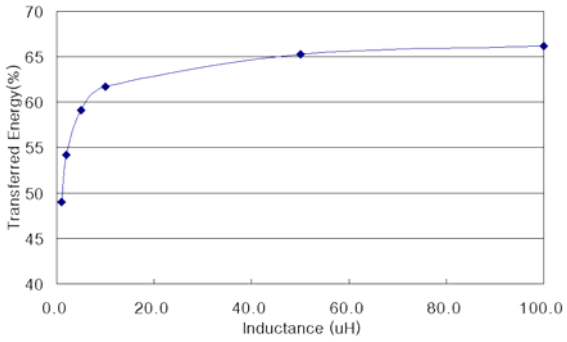

Fig. 9 Transferred energy to the battery versus the resonant inductance *L*

Fig. 9 shows that the inductor has a great effect on the efficiency of the converter. The bigger inductor makes the peak current smaller so that the ohmic loss will be reduced.

7. Experiments

The experiments are performed to prove the feasibility

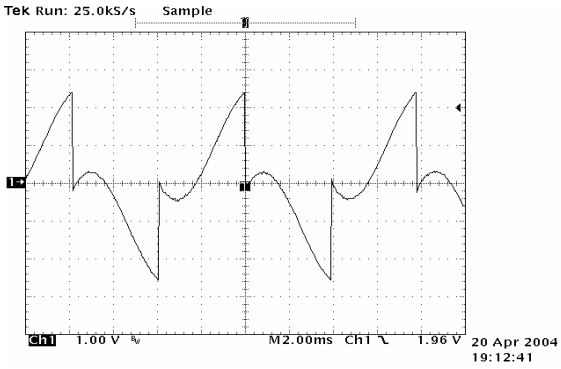

(a)

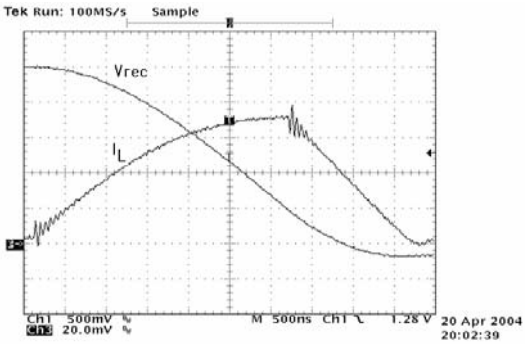

(b)

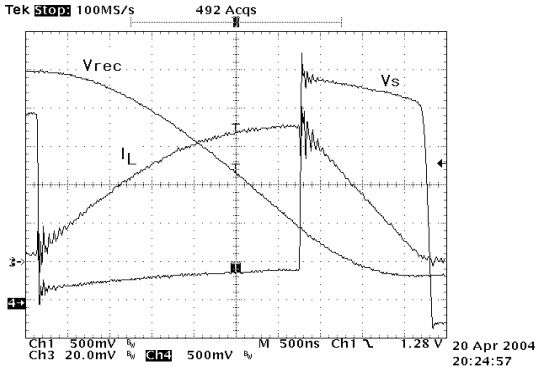

(c)

Fig. 10 Measured waveforms of the converter (a) V_{rec} on 1V/div and 2ms/div (b) V_{rec} (500mV/div) and I_L (16mA/div) on time scale 500ns/div (c) V_{rec} and V_S (500mV/div), I_L (16mA/div) on time scale 500ns/div

of the new converter for energy harvesting. A detailed explanation of the fabrication and test of the converter is in the referred paper[9]. In the experiment, the best-measured efficiency of the converter is slightly above 70% with 100 [μH] inductor. The measured efficiency approximately corresponds to the calculated efficiency of 67% in Fig 9.

Fig 10(a) shows the waveform of $V_{ab}(t)$ in Fig. 1, which is the same as Fig. 5(a). For comparison, Fig. 10(b) shows the current of the resonant inductor and the voltage of $V_{ab}(t)$ in the enlarged time scale. Fig. 10(c) shows the voltage of $V_S(t)$, the current of the resonant inductor and the voltage of $V_{ab}(t)$ in the enlarged time scale. The experimental results of the converter for energy harvesting closely corresponds to the analytical results.

8. Conclusions

A new AC/DC resonant pulse power converter for energy harvesting is proposed. In this paper, a PZT device, which is an energy source for energy harvesting, is simply modeled as an ideal current source in parallel with a capacitor. For compactness, the converter does not have a capacitor inside. The converter uses zero voltage switching and zero current switching with the LC_e resonance. The operation of the converter is analyzed with consideration of the parasitic capacitances of MOSFETs since the LC_e resonant frequency is too high. Eight operational modes of the converter are defined and the converter efficiencies versus the parasitic capacitance and the resonant inductance are calculated.

Simulation studies and simple experiments are performed to show the existence of eight operational modes, the realization of the control algorithm, and the efficiency of the converter. In this paper, the feasibility of the proposed converter for energy harvesting is proved.

Acknowledgment

This work was supported by a Korea Research Foundation Grant" (KRF-2003-013-D00047). The authors would like to thank Mr. ShengWen Xu and Dr. Toshikazu Nishida of the University of Florida for their help in the experiment.

References

[1] Geffrey K. Ottman, Health F. Hofmann, Archin C. Bhat, George A. Lesieutre, "Adaptive Piezoelectric Energy Harvesting Circuit for Wrieless Remote Power Supply,"

IEEE transactions on Power Eletronics, Vol. 17, No. 5, pp. 669 676, September 2002.

[2] Stephen Horowitz, Anurag Kasyap, Fei Liu, David Johnson, Toshi Nisida, Khai Ngo, Mark Sheplak, Louis Cattafesta, "Technology Development for Self-Powered Sensors," American Institute of Aeronautics and Astronautics, AIAA Paper-2002-2702, 1st Flow Control Conference, June 24-26, St. Louis, MO.

[3] Nathan S. Schenck, Joseph A. Paradiso, " Energy Scavenging with Shoe-Mounted Piezoelectrics, "IEEE Micro, Vol. 21, pp.30-42, May-June 2001.

[4] P. Glynne-Jones, S.P. Beeby, N.M. White, "Towards a piezoelectric vibration-powered micro generator, " IEE Proc.-Sci. Meas. Technol., Vol. 148, No. 2, March 2001.

[5] Sam Ben-Yaakov, Simon Lineykin, " Frequency Tracking to Maximum Powerof Piezoelectric Transformer HV Converters under Load Variation, " IEEE PESC, Vol. 2 pp. 23-27, June 2002.

[6] Anurag Kasyap, Ji-Song Lim, David Johnson, Stephen Horowitz, Toshikazu Nishida, Khai Ngo, Mark Sheplak, Louis Cattafesta, "Energy Reclamation from a Vibrating Piezoceramic Composite Beam," 9th International Congress on Sound and Vibration, ICSV9.

[7] Robert W. Erickson, Dragan Maksimovic, " Fundamentals of Power Electronics- 2nd Ed.," Kluwer Academic Publishers, 2001, ISBN: 0792372700.

[8] R. Blanchard, P.E. Thilbodeau, " The design of a high efficiency, low voltage power supply using MOSFET synchronous rectification and current mode control," Proceedings of IEEE PESC'85, 16th Annual Meeting, pp.355-361.

[9] Shengwen Xu, Khai Ngo, Toshikazu Nishida, Gyo-Bum Chung, Attma Sharma, "Converter and Controller for Micro-Power Energy Harvesting," accepted for IEEE APEC 2005 Conference.

Gyo-Bum Chung was born in Seoul, Korea, in 1959. He received B.S. and M.S. degrees in electrical engineering from Seoul National University, in 1983 and 1985, respectively, and a Ph.D. degree in electrical engineering from the University of Florida, Gainesville, FL, USA, in 1992. He was a research associate at VPI & SU, Blacksburg, VA, USA, from 1992 to 1993. He was a senior researcher for the electric vehicle development team at the Korea Electro-technology Research Institute from 1993 to 1994. Since 1995, he has been with the Department of Electronic and Electrical Engineering, Hongik University, where he is currently an associate professor. His research interests are in the areas of power electronics; the design of power converters, power quality, FACTS and advanced control of electrical machines. Prof. Chung is a member of the Korean Institute of Power Electronics.

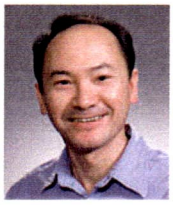

Khai D. T. Ngo received a B.S.E.E. degree from California State Polytechnic University, Pomona in 1979; M.S.E.E. and Ph.D. degrees from California Institute of Technology in 1980 and 1984, respectively. Prior to 1988, he was a Member of the Technical Staff at the GE Research and Development Center. He is a Professor of Electrical and Computer Engineering and has been at the University of Florida since 1988. His current research interests include the synthesis and control of power converters; power quality; low-profile magnetics; micropower conversion; power semiconductor devices and integrated circuits. Prof. Ngo is a senior member of the Institute of Electrical and Electronic Engineers.